

Photogalvanic currents from first-principles real-time density-matrix dynamics

Junting Yu,¹ Andrew Grieder,¹ Jacopo Simoni,¹ Rafi Ullah,¹ Zihao Bai,²
Ravishankar Sundararaman,³ Aris Alexandradinata,^{4,*} and Yuan Ping^{1,5,2,†}

¹*Department of Materials Science and Engineering, University of Wisconsin-Madison*

²*Department of Chemistry, University of Wisconsin-Madison*

³*Department of Materials Science and Engineering, Rensselaer Polytechnic Institute*

⁴*Department of Physics and Santa Cruz Materials Center, University of California, Santa Cruz*

⁵*Department of Physics, University of Wisconsin-Madison*

(Dated: March 10, 2026)

The photogalvanic effect is the generation of a second-order direct current by illumination of a non-centrosymmetric material. In this work, we develop a first-principles real-time density matrix (FPDMD) formalism enabling the calculations of the photogalvanic current in all time regimes: transient and steady. Unlike past *ab-initio* studies which focused only on the photo-excitation process, our first-principles theory framework encodes all quantum scatterings (intra/interband relaxation and electron-hole recombination) mediated by bosons (photons and phonons), and is thus predictive of photogalvanic currents in realistic materials. In particular, for the linear photogalvanic effect, we find electron scatterings mediated by phonons contribute significantly to the shift current for prototypical piezoelectrics like BaTiO₃. For the circular photogalvanic effect, we develop a self-consistent theory of a steady injection current that incorporates realistic scattering mediated by phonons. Our formulation developed for photogalvanic current elucidates its connection with fundamental quantum-geometric quantities such as the Berry curvature and the quantum metric. A phonon-based explanation is proposed for the bipolar transient photogalvanic current observed by the THz emission spectroscopy.

The photogalvanic effect (PGE), also known as the bulk photovoltaic effect, is the light-induced generation of a direct current in a homogeneous, non-centrosymmetric medium, without inhomogeneous doping or externally applied fields [1, 2]. Interest in the photogalvanic effect has resurged, owing to recently unveiled connections with the quantum geometry of electronic wave functions in topological materials [3–5] and superlattices. This has led to envisioned applications to polarization- and frequency-sensitive photodetectors, as well as efficient solar cells capable of harvesting light with photon energy below 1 eV [5]. Other applications of the PGE include the detection of centrosymmetry breaking in chiral and ferroelectric materials [6–10], the detection of spin-splitting due to Rashba/Dresselhaus spin-orbit interactions [11, 12], as well as tracking the ultrafast dynamics of electron distributions and order parameters [13–16].

Here we develop a first-principles real-time density matrix dynamics (FPDMD) formalism for the PGE, based on quantum master equations (QME) which encode all quantum kinetic scatterings mediated by bosons (photons and phonons), including not just the well-studied photo-excitation process but also the intra- and interband relaxations and the electron-hole recombinations illustrated in Fig. 1(a). Our theory is thus predictive of the photogalvanic current in realistic materials where electron-phonon scattering cannot be ignored, and promises to resolve controversy and confusion about the underlying scattering mechanisms that contribute to the current. Contrary to the common misconception that the shift photogalvanic current (generated in nonmagnetic systems under linearly polarized light) is purely a photo-

excitation effect, we demonstrate that phonon-mediated scattering will contribute significantly to the shift current in prototypical piezoelectrics. With first-principles real-time density matrix formalism, we go beyond prior model-Hamiltonian studies of PGE in topological materials [5], and we demonstrate that phonon contributions to the shift current are ubiquitous across piezoelectrics. Next, we develop a self-consistent theory of the steady photogalvanic current under circular polarized light, with a state-dependent relaxation time $\tau_{\mathbf{k}s}$ and the non-equilibrium steady electron distributions. This goes beyond previous perturbative calculations of the linear growth dJ/dt [17], where a single relaxation time approximation τ_0 does not self-consistently describe the multiple scattering mechanism in realistic materials. Lastly, despite recent investigations of the transient photogalvanic current through THz emission experiments [14, 18–20] and numerical simulations [21], a rigorous explanatory theory remains to be developed. Our FPDMD opens a unique pathway into transient photogalvanic currents with femtosecond resolution. In particular, the experimental observation [18] of a bipolar $J(t)$ is explained as a dynamical cross-over from a photo-excitation-dominated current to an electron-phonon-dominated current.

To set up these results, the total Hamiltonian for an electron-boson system

$$H_T = H_0^e + H_0^b + H' = \sum_i \varepsilon_i c_i^\dagger c_i + \sum_m \hbar\omega_m a_m^\dagger a_m + H'$$

is a sum of three terms: (i) H_0^e is the unperturbed single-particle electronic Hamiltonian with a Bloch basis computed from first-principles Kohn-Sham Density-

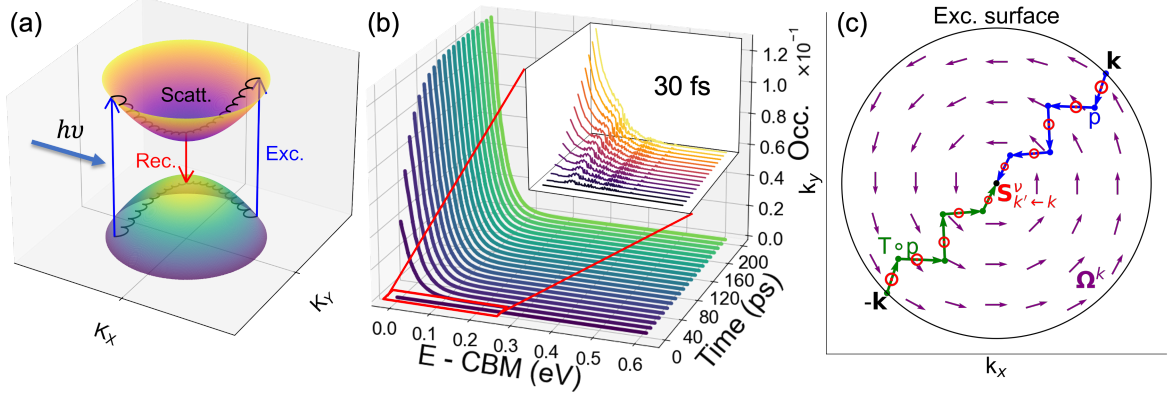


FIG. 1. Kinetic process and electron occupation under an external light illumination. (a) Kinetic processes including light excitation, scattering and recombination. (b) Excited carrier occupation changes with time in conduction bands within 200 ps; the inset zooms in the first 30 fs. The excitation peak is formed within 10 fs, but conduction electrons are then quickly scattered to conduction band edge. Within 25 fs (the energy relaxation time), the precursor of a quasi-Fermi-Dirac distribution forms, with a quasi temperature 315K. (c) For the conduction surface at $\hbar\omega - E_g = 0.32$ eV. Under electron-phonon scattering, the blue arrows (p) illustrate one representative electron trajectory from \mathbf{k} to band bottom, while the green arrows ($T \circ p$) is the trajectory that is the time-reverse of p . For a small-momentum scattering event from \mathbf{k} to \mathbf{k}' , the electron is displaced in real space by the phononic shift vector $\mathbf{S}_{\mathbf{k}' \leftarrow \mathbf{k}}^{\nu} = \mathbf{\Omega}^{\mathbf{k}} \times (\mathbf{k}' - \mathbf{k})$ with $\bar{\mathbf{k}} = (\mathbf{k} + \mathbf{k}')/2$. This cross product of a purple arrow and a blue/green arrow is represented as a red circle and points in the z direction, which is the polar axis of BaTiO₃. The shift contributions from p and $T \circ p$ add up instead of canceling out, because under time-reversal, $\mathbf{\Omega}^{-\bar{\mathbf{k}}} = -\mathbf{\Omega}^{\bar{\mathbf{k}}}$ and $(\mathbf{k} - \mathbf{k}') = -(\mathbf{k}' - \mathbf{k})$, leaving the shift vector invariant.

Functional Theory (KSDFFT) and $c_i = c_{\mathbf{k},s}$ annihilates an electron with wavevector \mathbf{k} and band label s . (ii) H_0^b is the unperturbed boson Hamiltonian, and a_m annihilates a boson (phonon or photon) with mode index m . (iii) The interaction Hamiltonian is

$$H' = \sum_m \sum_{ij} \lambda_{ij}^m c_i^\dagger c_j \otimes (a_m + a_{-m}^\dagger), \quad (1)$$

where λ_{ij}^m is the electron-boson interaction matrix element:

$$\lambda_{ij}^m = \begin{cases} \delta_{\mathbf{k}_i, \mathbf{k}_j + \mathbf{q}} \sqrt{\frac{e^2 \hbar}{2\epsilon_0 \omega V}} \mathbf{e} \cdot \mathbf{v}_{s_i, \mathbf{k}_j}^{\mathbf{k}_i, \mathbf{k}_j}, & m = (\mathbf{e}, \mathbf{q}) \text{ for photon} \\ \delta_{\mathbf{k}_i, \mathbf{k}_j + \mathbf{q}} g_{s_i s_j}^{\nu, \mathbf{k}_i, \mathbf{k}_j}, & m = (\nu, \mathbf{q}) \text{ for phonon.} \end{cases}$$

Focusing first on the electron-photon interaction, we use velocity gauge, $\mathbf{v}_{s_i, \mathbf{k}_j}^{\mathbf{k}_i, \mathbf{k}_j} = \langle \phi_{\mathbf{k}_i, s_i} | e^{i\mathbf{q} \cdot \mathbf{r}} \mathbf{v} | \phi_{\mathbf{k}_j, s_j} \rangle$, with $\phi_{\mathbf{k}_i, s_i}$ being single particle wavefunctions, $\mathbf{v} = \frac{i}{\hbar} [\mathbf{r}, H_0^e]$ being the velocity operator and H_0^e including the non-local part of the atomic pseudopotential in KSDFFT. We consider direct optical transitions in the dipole approximation at long wavelength limit $\mathbf{q} \rightarrow 0$. If we assume the light source is monochromatic with a classical electromagnetic vector potential, the electron-photon interaction will be connected with vector potential via $\lambda_{ij}^m = \delta_{\mathbf{k}_i, \mathbf{k}_j} (e/2\sqrt{N}) \mathbf{A}_0 \cdot \mathbf{v}_{s_i, s_j}^{\mathbf{k}_i, \mathbf{k}_j}$ with $\mathbf{A}_0 = \sqrt{2\hbar N / (\epsilon_0 \omega V)} \mathbf{e}$ the amplitude of light vector potential, \mathbf{e} the light polarization vector (which may be real for linearly-polarized light and must be complex for circularly-polarized light),

and N the light-source photon occupation number. For the electron-phonon interaction, $\delta_{\mathbf{k}_i, \mathbf{k}_j + \mathbf{q}}$ is the momentum conservation constraint, and $g_{s_i s_j}^{\nu, \mathbf{k}_i, \mathbf{k}_j}$ is the first-order electron-phonon matrix element (for a phonon eigenmode ν) computed from density-functional perturbation theory [22–24].

The QME describes the time evolution of the electron reduced density-matrix (RDM) accounting for photoexcitation (exc), electron-phonon scattering (ph) and electron-hole recombination (rec) processes [25–27]:

$$\frac{d\rho}{dt} = -\frac{i}{\hbar} [H_0^e, \rho] + \frac{d\rho}{dt}|_{\text{exc}} + \frac{d\rho}{dt}|_{\text{ph}} + \frac{d\rho}{dt}|_{\text{rec}}. \quad (2)$$

While in principle time-dependent electron-electron scattering can also influence RDM dynamics (discussed in our work on open quantum dynamics formulation [26] and ultrafast spin dynamics [25]), in practice it is only relevant at low temperature [27, 28] or high-intensity light sources [29], which we avoid in this work. The charge current density is evaluated as $\mathbf{J}(t) = -e \text{Tr}(\rho(t) \mathbf{v}) = \sum_{n=0}^{+\infty} J(\omega) e^{in\omega t}$, with different Fourier components giving the direct current ($n = 0$), second ($n = 2$), and higher harmonic generation. It is useful to decompose $\mathbf{J} = \mathbf{J}^d + \mathbf{J}^{\text{off}}$, such that the band-diagonal current \mathbf{J}^d (band-off-diagonal current \mathbf{J}^{off}) is contributed by the band-diagonal (resp. band-off-diagonal) matrix elements of ρ . Other types of current can be obtained by evaluating the corresponding observable, e.g. the spin photocurrent density $\mathbf{J}_S(t) = \text{Tr}(\rho(t)(\mathbf{S}\mathbf{v} + \mathbf{v}\mathbf{S})/2)$ [30, 31].

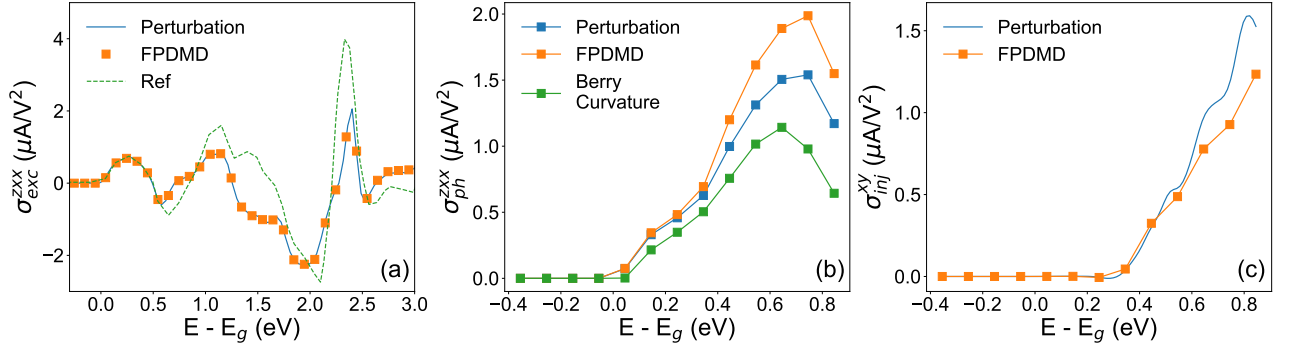


FIG. 2. Different DC photocurrent conductivities of BaTiO₃. (a) Excitation shift current conductivity in xxx direction. Real time result is from evaluating the steady-state off-diagonal part of the density matrix, with eliminating other contributions except excitation current. Reference data is from Ref.[32]. (b) Phonon shift current conductivity from perturbation theory, FPDMD, and Berry curvature formula at RT in xxx direction. FPDMD is obtained by eliminating other contributions except phonon shift current. Perturbation refers to results calculated by Eq.(4). The Berry curvature results are obtained by replacing $\mathbf{S}_{\mathbf{k}'s \leftarrow \mathbf{k}s}^\nu$ with $\mathbf{q} \times \boldsymbol{\Omega}_{ss}^\mathbf{k}$, and only considering intra-band electron-phonon scattering in Eq.4. (c) Injection current conductivity of BaTiO₃ from perturbation theory (Eq. 6) and FPDMD. The perturbation result uses state-dependent electron-phonon relaxation rate (Eq. 7).

Under the Born-Markov approximation, the QME of electron-boson interaction has the following form [33, 34],

$$\left. \frac{d\rho_{12}}{dt} \right|_c = \sum_{345} (I - \rho)_{13} \rho_{45} P_{3245}^c - \rho_{32} (I - \rho)_{45} P_{5431}^c + (1 \leftrightarrow 2)^* \quad (3)$$

$$P_{1234}^c = \frac{\pi}{\hbar} \sum_{m \in c, \pm} N_m^\mp \Lambda_{13}^{\pm m \mp} \lambda_{24}^{\pm m *},$$

for each scattering channel $c = exc, ph, rec$; $\Lambda_{12}^{\pm} = \lambda_{12}^m \delta(\varepsilon_1 - \varepsilon_2 \pm \hbar\omega_m)$, $N_m^\pm = N_m + \frac{1}{2} \pm \frac{1}{2}$, and N_m are boson occupations.

Our case study focuses on tetragonal BaTiO₃, a prototypical piezoelectric with a long history of non-linear optical measurements [35–39]. Fig. 1 presents the carrier dynamics of this system from FPDMD: (b) shows that within 10 fs of turning on the light source, the electrons form a peak located around the excitation energy $\varepsilon_{\mathbf{k}c} = \varepsilon_{\mathbf{k}v} + \hbar\omega \approx 1.9$ eV. Within 30 fs, close to the energy relaxation time $\tau_{er} = 25$ fs in Fig. 4, electrons are scattered to the conduction band edge, and the aforementioned excitation peak evolves to a cusp (Fig. 1(b) inset). Within several hundred ps, a quasi-Fermi-Dirac distribution develops for electrons and holes respectively, with a common fitted temperature $T = 315$ K, which is close to the phonon temperature of 300 K.

Focusing first on the PGE under linearly-polarized light, we isolate the *excitation shift current* \mathbf{J}_{exc}^{sh} by implementing the relaxation time approximation (RTA) for other processes except excitation: $d\rho/dt|_{ph} + d\rho/dt|_{rec} = -(\rho - \rho^{eq})/\tau_0$ for electron-phonon scattering and recombination processes, which effectively eliminates their contributions to the shift current [40]. In the steady state, the band-off-diagonal current is identified as $\mathbf{J}^{off} = \mathbf{J}_{exc}^{sh}$. The second-order photocurrent conductivity tensor is then calculated as $\sigma_{exc}^{abc} = \mathbf{J}_a^{off}/E_b(\omega)E_c(-\omega)$, with

$E_b(\omega) = i\omega A_b$ being the electric field. Fig. 2(a) shows our real-time-simulated \mathbf{J}_{exc}^{sh} agrees with the perturbative formula [17, 41], validating our FPDMD method for calculating non-linear photocurrents.

Crucially, the phonon contribution to the shift current, which is missing in the aforementioned RTA, can only be calculated when explicit electron-phonon scattering is included in the QME. We extract this *phonon shift current* \mathbf{J}_{ph}^{sh} by subtracting the excitation shift current and recombination current from FPDMD total current. Fig. 2(b) shows a semi-quantitative agreement between our FPDMD phonon-shift current and the perturbative, steady-state formula[42]:

$$\mathbf{J}_{ph}^{sh;pert} = \frac{2e\pi}{\hbar V} \sum_{\mathbf{k}\mathbf{k}'s's'\nu} \mathbf{S}_{\mathbf{k}'s' \leftarrow \mathbf{k}s}^\nu |g_{ss'}^{\nu\mathbf{k}\mathbf{k}'}|^2 \delta(\varepsilon_{\mathbf{k}s} - \varepsilon_{\mathbf{k}'s'} + \hbar\omega_{\mathbf{q}\nu}) \times [(N_{\mathbf{q}\nu} + 1)(1 - f_{\mathbf{k}s})f_{\mathbf{k}'s'} - N_{\mathbf{q}\nu}(1 - f_{\mathbf{k}'s'})f_{\mathbf{k}s}], \quad (4)$$

where $\mathbf{S}_{\mathbf{k}'s' \leftarrow \mathbf{k}s}^\nu$ is the phononic shift vector, $\mathbf{q} = \mathbf{k} - \mathbf{k}'$ is the phonon momentum, and $N_{\mathbf{q}\nu} = 1/(e^{\beta\hbar\omega_{\mathbf{q}\nu}} - 1)$ is the thermal phonon occupation. Fig. 3(b) shows that \mathbf{J}_{ph}^{sh} is comparable in magnitude to \mathbf{J}_{exc}^{sh} at low light frequencies, but becomes dominant at higher light frequencies. This is because \mathbf{J}_{exc}^{sh} is contributed only by one-electron states near the excitation \mathbf{k} -surface (defined by $\varepsilon_{\mathbf{k}c} - \varepsilon_{\mathbf{k}v} = \hbar\omega$); at higher frequencies, the excitation \mathbf{k} -surface encloses a larger volume of one-electron states whose mutual scatterings contribute to the phonon shift current [5].

For intraband electron-phonon scatterings at small \mathbf{q} , the phonon shift vector reduces to $\mathbf{S}_{\mathbf{k}'s' \leftarrow \mathbf{k}s}^\nu = \mathbf{q} \times \boldsymbol{\Omega}_{ss}^\mathbf{k} + O(q^3)$ [5], with $\mathbf{k} = (\mathbf{k} + \mathbf{k}')/2$, and the intraband Berry curvature $\boldsymbol{\Omega}^\mathbf{k} = \nabla_{\mathbf{k}} \times \boldsymbol{\xi}^\mathbf{k}$ being the curl of the intraband Berry connection $\boldsymbol{\xi}_{ss}^\mathbf{k} = i\langle u_{\mathbf{k}s} | \nabla_{\mathbf{k}} u_{\mathbf{k}s} \rangle$, with $u_{\mathbf{k}s}$ being the periodic part of single particle wavefunctions. By approximating the phonon shift vectors in Eq. (4) by their

intraband Berry curvature formula, we obtain the approximate phonon shift current [green curve in Fig. 2(b)] that is semi-quantitatively consistent with the real time FPDMD current, indicating the prevalence of small- \mathbf{q} scattering and validating the quantum-geometric PGE theory [5]. As explained under Fig. 1(c), the circulation of the Berry curvature is intimately tied to the ferroelectricity in BaTiO₃; to flip the circulation (from anticlockwise to clockwise) is to invert the direction of J_{ph}^{sh} along the polar axis.

To compare our real-time, steady-state PGE with the experimental data on BaTiO₃ under linear light, we calculate the DC photocurrent as [32, 36, 43]

$$\text{Current}(abb) = \frac{\sigma_{abb}(\omega)}{\alpha_{bb}(\omega)}(1 - R_{bb}(\omega))L \cdot |E_b(\omega)|^2, \quad (5)$$

with α_{bb} being the absorption coefficient, R_{bb} the reflectivity, L the sample width, and E_b the electric field amplitude along the b direction. The comparison among excitation shift current, total current from FPDMD, and the experimental result is shown in Fig. 3(a). The excitation shift current is similar to the past perturbation theory result [32]. It alone underestimates photocurrent compared with experiments, which is large between 0.0 and 0.6 eV above the band edge transition. Past work based on phonon-assisted ballistic current represents a different phonon-mediated mechanism from this work [44]. It enhances photocurrent between 0.0 and 0.2 eV, improved agreement with experiments[44]. Our phonon contribution brings total photocurrent closer to experiments in a wider range of energy above the band edge transition. The improved agreement with experiments from both studies indicates that phonon-mediated scatterings plays a significant role in the PGE.

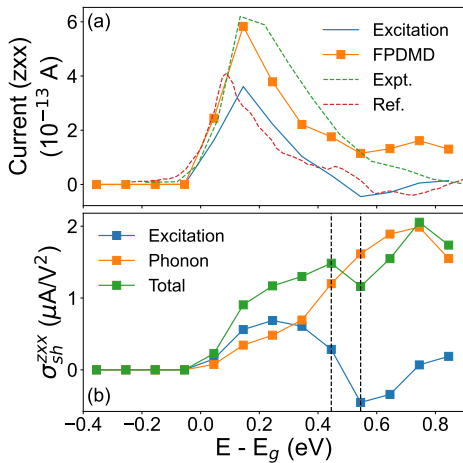


FIG. 3. Photogalvanic current and conductivity of BaTiO₃ in zxx direction. (a) Comparison of photocurrent (Eq. 5) from real-time FPDMD, experiment result [37] and reference work [44]. (b) The total shift current conductivity and separate current components from FPDMD.

Under circularly-polarized light excitation, the injection current \mathbf{J}^{inj} is identified with the band-diagonal \mathbf{J}^d calculated from FPDMD, and compared with the perturbative expression for the steady injection current density developed in this work due to photo-excitation:

$$\mathbf{J}^{inj;pert} = i \frac{\pi e^3}{2\hbar V} |A_0|^2 \sum_{\mathbf{k}} \sum_{ss'} f_{ss'}^{\mathbf{k}} (\tau_{\mathbf{k}s} \mathbf{v}_{ss}^{\mathbf{k}} - \tau_{\mathbf{k}s'} \mathbf{v}_{s's'}^{\mathbf{k}}) \times (v_{s's}^{bk} v_{ss'}^{ck} - v_{s's}^{ck} v_{ss'}^{bk}) \delta(\varepsilon_{ss'}^{\mathbf{k}} - \hbar\omega), \quad (6)$$

which we derive in SI III.A. Here, A_0 is the amplitude of the vector potential: $\mathbf{A}(t) = \frac{1}{2} A_0 [\exp(-i\omega t) \mathbf{e} + \exp(i\omega t) \mathbf{e}^*]$, $\mathbf{e} = \mathbf{e}_b + i\mathbf{e}_c$ is the complex polarization vector, $f_{ss'}^{\mathbf{k}} = f_{\mathbf{k}s} - f_{\mathbf{k}s'}$ is occupation difference between two bands, and $\tau_{\mathbf{k}s}$ is a state-dependent relaxation time. Assuming that the carrier relaxation is dominated by electron-phonon scattering at room temperature, which is typical for most semiconductors [23, 27], we relate the inverse relaxation time to the electron-phonon carrier lifetime [25, 45],

$$\frac{1}{\tau_{\mathbf{k}s}} = \frac{2\pi}{\hbar} \sum_{\mathbf{k}'s'} \sum_{\nu\pm} (N_{\mathbf{q}\nu}^{\mp} \pm f_{\mathbf{k}'s'}) \delta(\varepsilon_{\mathbf{k}s} - \varepsilon_{\mathbf{k}'s'} \pm \hbar\omega_{\mathbf{q}\nu}) |g_{ss'}^{\nu\mathbf{k}\mathbf{k}'}|^2. \quad (7)$$

Here, $f_{\mathbf{k}'s'}$ is the steady electron distribution (photoexcited under light illumination, i.e. Fig. 1(b)), obtained from our FPDMD and input to Eqs. (6)-(7), which represents a self-consistent solution. In previous, heuristic estimations of injection current[4, 46, 47], it is a common practice to replace the state-dependent $\tau_{\mathbf{k}s}$ by a state-independent relaxation time τ_0 , and $f_{\mathbf{k}s}$ by the equilibrium electron Fermi-Dirac distribution in the dark. The injection current conductivity can be calculated via $J_a^{inj} = 2\sigma_{inj}^{ab} [\mathbf{E}(\omega) \times \mathbf{E}^*(-\omega)]_b$. We focus on the σ_{inj}^{xy} component, the largest one for BaTiO₃. Fig. 2(c) shows this conductivity in reasonably good agreement between the FPDMD and the perturbative formula in Eqs. (6)-(7).

In the limit of a single conduction and a single valence band, the injection current conductivity in Eqs. (6)-(7) can be reformulated in terms of the Berry curvature Ω^{bk} :

$$\sigma_{ab}^{inj} = \frac{\pi e^3}{2\hbar V} \sum_{\mathbf{k}} \Omega_{11}^{bk} (\tau_{\mathbf{k}1} v_{11}^{ak} - \tau_{\mathbf{k}2} v_{22}^{ak}) \delta(\varepsilon_{\mathbf{k}12} - \hbar\omega). \quad (8)$$

Here 1 and 2 represent conduction and valence band indices respectively. If $\tau_{\mathbf{k}1}$ is dominated by small- \mathbf{q} , intraband electron-optical-phonon scattering, we may identify $|g_{ss}^{\nu\mathbf{k}\mathbf{k}'}|^2 = \kappa_{\nu} (1 - \sum_{ij} q_i q_j \zeta_{\mathbf{k}s}^{ij}) / q^2$ [5], with κ_{ν} being a non-zero constant for longitudinal optical (LO) phonons, and $\zeta_{\mathbf{k}s}^{ij} = \text{Re} \langle \nabla_{\mathbf{k}}^i u_{\mathbf{k}s} | \nabla_{\mathbf{k}}^j u_{\mathbf{k}s} \rangle - \zeta_{ss}^{ik} \zeta_{ss}^{jk}$ being the quantum metric [48]. Thus, Eqs. (7)-(8) elegantly synthesize two fundamental quantum geometric characteristics which relate to two separate kinetic processes: the Berry curvature of one-electron states on the photo-excitation surface (as was emphasized heuristically in Ref. [4]), and

the quantum metric of one-electron states related by intraband electron-phonon scattering.

To simulate the transient photogalvanic current measured in recent ultrafast THz emission spectroscopy [14, 18, 49–51], we perform FPDMD for the transient shift current, by applying a linearly-polarized light pump $I(t) \propto \exp[-(t/\bar{\tau})^2]$ centered at $t = 0$ with width $\bar{\tau} = 20$ fs and measuring the response current. The transient excitation, phonon and total shift current responses of BaTiO₃ from FPDMD are shown in Fig. 4 at two light frequencies. The J_{exc} , excitation-shift current, responds quickly to the pulse, with a time lag $\tau_{eph} = 0.75$ fs that has the same magnitude as the electron-phonon scattering time. The J_{ph} , phonon-shift current, responds with a time lag $\tau_{er} \approx 25$ fs, close to the energy relaxation time, which is approximately the time that photoexcited electrons are scattered from the excitation surface to the band extrema [52]. The time lags $\tau_{eph/er}$ of $J_{exc/ph}$ are respectively quantified by fitting each FPDMD-derived current to a time convolution of a Kernel function ($K_{exc}(t)$ or $K_{ph}(t)$) and the light intensity ($I(t)$). Here, each $K(t)$ is exponentially decaying with a decay constant equal to the corresponding time lag: $K(t) \propto \exp[-t/\tau]$, as detailed in SI Sec. IV. The two different time lags result in the total transient current being (a) bipolar when J_{exc} and J_{ph} have different signs, and (b) unipolar when J_{exc} and J_{ph} have the same sign. Our theory thus predicts a photon-frequency-dependent crossover between unipolar and bipolar $J(t)$, which possibly explains the puzzlingly bipolar $J(t)$ observed in THz emission spectroscopy of a number of systems [14, 18–20].

In summary, we develop a first-principles real-time density matrix dynamics formalism for calculating the photogalvanic effect (PGE), enabling one to obtain different contributions from a unified theoretical framework. Taking BaTiO₃ as an example, we reproduce the excitation shift current and injection current that are consistent with perturbative methods. With explicit electron-phonon scattering, we find significant phonon shift current at excited states. Besides steady state DC, we are able to study the transient current that is directly accessible during the real time simulation, enabling us to understand photocurrent response in ultrafast THz spectroscopy experiments. Our work provides a general theoretical framework to study other contributions such as Coulomb scattering and higher-order scattering processes in the future [21, 54, 55]. Other non-linear optics such as second harmonic generation (SHG) or higher-order harmonic generation (HHG) can be extracted straightforwardly from this theory [56], which is important for characterization of topological properties and novel quantum materials. Beyond the charge photocurrent, other observables can be readily evaluated, e.g. the spin photocurrent [30, 57] and orbital photocurrent [58], which recently sparked interest in the spin-optoelectronic and orbitronics [59, 60] community.

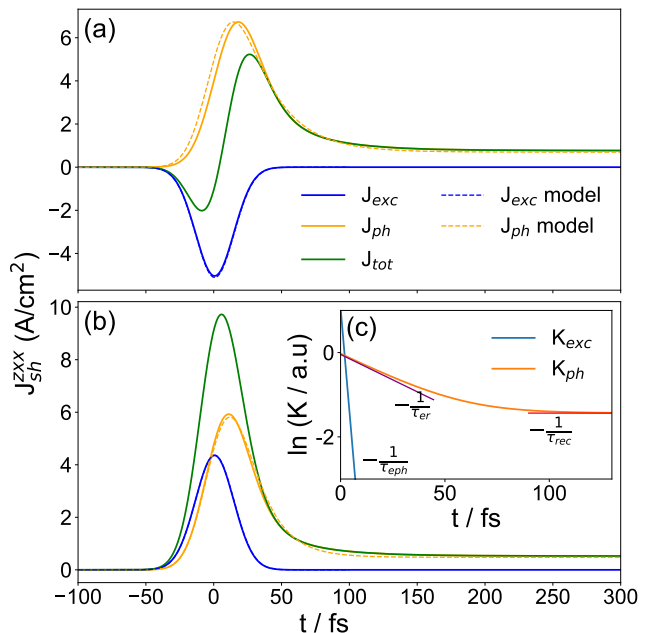


FIG. 4. FPDMD simulation of $J(t)$ and their kernel-modeled results for BaTiO₃, using a Gaussian light pulse centered at $t = 0$ with width 20 fs. The modeled results are fitted against FPDMD. Whether $J(t) = J_{tot}(t)$ is bipolar [as in panel (a) with photon energy at $0.545eV + E_g$] or unipolar [panel (b) with photon energy at $0.445eV + E_g$] is determined by whether the steady-state excitation and phonon shift currents have opposite sign [the second dashed line in Fig. 3(b)] or the same sign [the first dashed line in Fig. 3(b)]. Panel (c) shows the fitting of real time dynamics to the convolution of $I(t)$ and $K(t)$ (kernel-models), where three different time scales are obtained, roughly in agreement with the electron-phonon scattering time τ_{eph} , energy relaxation time τ_{er} , and recombination time τ_{rec} of this system [53] (Details in SI Sec. IV).

Acknowledgments We thank Junqing Xu, Elio J Koenig, and Liang Tan for very helpful discussions. This work is primarily supported by the Computational Chemical Sciences program within the Office of Science of the DOE under Grant No. DE-SC0023301. Part of the work is supported by the Air Force Office of Scientific Research under Award No. FA9550-21-1-0087. Calculations were carried out at the National Energy Research Scientific Computing Center (NERSC), a U.S. Department of Energy Office of Science User Facility operated under Contract No. DEAC02-05CH11231.

* aalexan6@ucsc.edu

† yping3@wisc.edu

- [1] V. I. Belinicher and B. I. Sturman, Soviet Physics Uspekhi **23**, 199 (1980).
- [2] V. Fridkin, Crystallography Reports **46**, 654 (2001).
- [3] L. Z. Tan and A. M. Rappe, Physical review letters **116**, 237402 (2016).
- [4] F. De Juan, A. G. Grushin, T. Morimoto, and J. E.

- Moore, Nature communications **8**, 15995 (2017).
- [5] P. Zhu and A. Alexandradinata, Physical Review B **110**, 115108 (2024).
- [6] Q. Ma, S.-Y. Xu, C.-K. Chan, C.-L. Zhang, G. Chang, Y. Lin, W. Xie, T. Palacios, H. Lin, S. Jia, *et al.*, Nature Physics **13**, 842 (2017).
- [7] C. Le and Y. Sun, Journal of Physics: Condensed Matter **33**, 503003 (2021).
- [8] Y. Li, J. Fu, X. Mao, C. Chen, H. Liu, M. Gong, and H. Zeng, Nature communications **12**, 5896 (2021).
- [9] A. Zenkevich, Y. Matveyev, K. Maksimova, R. Gaynutdinov, A. Tolstikhina, and V. Fridkin, Physical Review B **90**, 161409 (2014).
- [10] P. Feng, Z. Gong, B. Wang, Z. Wang, H. Xu, L. Zou, C. Liu, X. Han, Y. Cheng, B. Yu, *et al.*, Nature Communications **16**, 9839 (2025).
- [11] A. McConnell, S. Wang, A. Grieder, Y. Ping, D. B. Mitzi, and D. Sun, Advanced Functional Materials , e21735 (2025).
- [12] A. Grieder, S. Tu, and Y. Ping, Advanced Optical Materials , e01190 (2025).
- [13] J. Pettine, P. Padmanabhan, N. Sirica, R. P. Prasankumar, A. J. Taylor, and H.-T. Chen, Light: Science & Applications **12**, 133 (2023).
- [14] M. Sotome, M. Nakamura, J. Fujioka, M. Ogino, Y. Kaneko, T. Morimoto, Y. Zhang, M. Kawasaki, N. Nagaosa, Y. Tokura, *et al.*, Proceedings of the National Academy of Sciences **116**, 1929 (2019).
- [15] Y. Okamura, T. Morimoto, N. Ogawa, Y. Kaneko, G.-Y. Guo, M. Nakamura, M. Kawasaki, N. Nagaosa, Y. Tokura, and Y. Takahashi, Proceedings of the National Academy of Sciences **119**, e2122313119 (2022).
- [16] S. Subedi, W. Liu, W. Fang, C. Fox, Z. Zhai, F. Fei, Y. Ping, B. Lv, and J. Xiao, Advanced Optical Materials , 2403471 (2025).
- [17] J. Sipe and A. Shkrebtii, Physical Review B **61**, 5337 (2000).
- [18] L. Braun, G. Mussler, A. Hruban, M. Konczykowski, T. Schumann, M. Wolf, M. Müntenberg, L. Perfetti, and T. Kampfrath, Nature communications **7**, 13259 (2016).
- [19] M. Sotome, M. Nakamura, J. Fujioka, M. Ogino, Y. Kaneko, T. Morimoto, Y. Zhang, M. Kawasaki, N. Nagaosa, Y. Tokura, *et al.*, Applied Physics Letters **114** (2019).
- [20] M. Sotome, M. Nakamura, T. Morimoto, Y. Zhang, G.-Y. Guo, M. Kawasaki, N. Nagaosa, Y. Tokura, and N. Ogawa, Physical Review B **103**, L241111 (2021).
- [21] L. Z. Tan, X. Andrade, S. Rajpurohit, A. A. Correa, and T. Ogitsu, arXiv preprint arXiv:2408.06320 (2024).
- [22] S. Baroni, S. de Gironcoli, A. Dal Corso, and P. Gianozzi, Rev. Mod. Phys. **73**, 515 (2001).
- [23] F. Giustino, Rev. Mod. Phys. **89**, 015003 (2017).
- [24] For more details see SI sec IV.
- [25] J. Xu and Y. Ping, J. Chem. Theory Comput. **20**, 492 (2024).
- [26] J. Simoni, G. Riva, and Y. Ping, J. Chem. Phys. , in press (2025).
- [27] J. Xu, A. Habib, R. Sundararaman, and Y. Ping, Phys. Rev. B Condens. Matter **104**, 184418 (2021).
- [28] J. Xu, K. Li, U. N. Huynh, M. Fadel, J. Huang, R. Sundararaman, V. Vardeny, and Y. Ping, Nature Communications **15**, 188 (2024).
- [29] S. Esipov and Y. Levinson, Advances in Physics **36**, 331 (1987).
- [30] H. Xu, H. Wang, J. Zhou, and J. Li, Nature Communications **12**, 4330 (2021).
- [31] T. Song, E. Anderson, M. W.-Y. Tu, K. Seyler, T. Taniguchi, K. Watanabe, M. A. McGuire, X. Li, T. Cao, D. Xiao, *et al.*, Science advances **7**, eabg8094 (2021).
- [32] R. Fei, L. Z. Tan, and A. M. Rappe, Physical Review B **101**, 045104 (2020).
- [33] H.-P. Breuer and F. Petruccione, *The theory of open quantum systems* (OUP Oxford, 2002).
- [34] R. Rosati, R. C. Iotti, F. Dolcini, and F. Rossi, Physical Review B **90**, 125140 (2014).
- [35] A. Von Hippel, Reviews of Modern Physics **22**, 221 (1950).
- [36] M. Cardona, Physical Review **140**, A651 (1965).
- [37] W. Koch, R. Munser, W. Ruppel, and P. Würfel, Solid State Communications **17**, 847 (1975).
- [38] S. Ehsan, M. Arrigoni, G. K. H. Madsen, P. Blaha, and A. Tröster, Physical Review B **103**, 094108 (2021).
- [39] V. Dwij, B. K. De, G. Sharma, D. Shukla, M. Gupta, R. Mittal, and V. Sathe, Physica B: Condensed Matter **624**, 413381 (2022).
- [40] More details can be found in SI sec II.A.
- [41] R. von Baltz and W. Kraut, Physical Review B **23**, 5590 (1981).
- [42] V. Belinicher, E. Ivchenko, and B. Sturman, Zh. Eksp. Teor. Fiz **83**, 649 (1982).
- [43] More details can be found in SI sec VI.
- [44] Z. Dai, A. M. Schankler, L. Gao, L. Z. Tan, and A. M. Rappe, Physical review letters **126**, 177403 (2021).
- [45] F. Giustino, Reviews of Modern Physics **89**, 015003 (2017).
- [46] L. Gao, Z. Addison, E. Mele, and A. M. Rappe, Physical Review Research **3**, L042032 (2021).
- [47] Z. Dai and A. M. Rappe, Chemical Physics Reviews **4** (2023).
- [48] J. Provost and G. Vallee, Communications in Mathematical Physics **76**, 289 (1980).
- [49] D. Kaplan, T. Holder, and B. Yan, Physical Review Research **4**, 013209 (2022).
- [50] M. Tong, Y. Hu, W. He, X.-L. Yu, S. Hu, X. Cheng, and T. Jiang, ACS nano **15**, 17565 (2021).
- [51] C. Somma, K. Reimann, C. Flytzanis, T. Elsaesser, and M. Woerner, Physical review letters **112**, 146602 (2014).
- [52] M. Lundstrom, Measurement Science and Technology **13**, 230 (2002).
- [53] The three timescales from fitting kernel models to FPDMD are $\tau_{eph} = 0.75$ fs, $\tau_{er} = 25$ fs, and $\tau_{rec} = 23$ ps. Here τ_{eph} is close to $\langle\tau_{ks}\rangle = 1.4$ fs, the averaged electron-phonon relaxation time over the excitation surface; τ_{er} is close to the time that excited electrons are scattered from excitation surface to band extrema, $\tau_{er} \approx \langle\tau_{ks}(\epsilon_{ks} - \epsilon_{CBM})/\hbar\omega_{LO}\rangle = 21.2$ fs, where $\omega_{LO} = 21.7$ meV is the energy of the dominant LO mode; τ_{rec} is consistent with experimental observed recombination lifetime ranging from 10ps to 100ps for different, impurity-varying samples of BaTiO₃.
- [54] Y.-H. Chan, D. Y. Qiu, F. H. da Jornada, and S. G. Louie, Proceedings of the National Academy of Sciences **118**, e1906938118 (2021).
- [55] N.-E. Lee, J.-J. Zhou, H.-Y. Chen, and M. Bernardi, Nature communications **11**, 1607 (2020).
- [56] M. Lewenstein, P. Balcou, M. Y. Ivanov, A. L’huillier, and P. B. Corkum, Physical Review A **49**, 2117 (1994).

- [57] T. Song, E. Anderson, M. W.-Y. Tu, K. Seyler, T. Taniguchi, K. Watanabe, M. A. McGuire, X. Li, T. Cao, D. Xiao, W. Yao, and X. Xu, *Science Advances* **7**, eabg8094 (2021), <https://www.science.org/doi/pdf/10.1126/sciadv.abg8094>.
- [58] X. Mu, Y. Pan, and J. Zhou, *Npj Comput. Mater.* **7**, 1 (2021).
- [59] D. Go, D. Jo, H.-W. Lee, M. Kläui, and Y. Mokrousov, *Europhysics Letters* **135**, 37001 (2021).
- [60] T. G. Rappoport, *Nature* **619**, 38 (2023).